Molecular dynamics investigation of the fracture behavior of nanocrystalline α-Fe

A. Latapie and D. Farkas
Department of Materials Science and Engineering, Virginia Polytechnic Institute and State University, Blacksburg, Virginia 24061-0237, USA
(Received 8 August 2002; published 21 April 2004)

We carried out classical atomistic studies of crack propagation in fully three-dimensional nanocrystalline α-Fe (body-centered cubic structure) to examine the influence of temperature and average grain size on the fracture mechanisms and properties. Digital samples with grain sizes ranging from 6 to 12 nm are reported at temperatures ranging from 100 K to 600 K using atomistic simulations. For all grain sizes, a combination of intragranular and intergranular fracture is observed. Mechanisms such as grain boundary accommodation, grain boundary triple junction activity, grain nucleation and grain rotation are observed to dictate the plastic deformation energy release. Intergranular fracture is shown to proceed by the coalescence of nanovoids formed at the grain boundaries ahead of the crack. The simulations also show that at an atomistic scale the fracture resistance and plastic deformation energy release mechanisms increase with increasing temperature. The observed fracture toughness increases with decreasing grain size.

DOI: 10.1103/PhysRevB.69.134110 PACS number(s): 62.20.Mk

I. INTRODUCTION

In the last two decades, grain-size refinement in polycrystalline metals has been the subject of intensive research. These materials with reduced grain sizes have been found to exhibit novel and often improved mechanical properties. On a very basic level, grain-size refinement associated with an increase in the amount of grain boundaries can make crack propagation more difficult and, therefore, in conventional grain size materials, increase the apparent fracture toughness. Thus, through reduction in grain-size, improved toughness can be achieved, in a similar way as an increase in yield strength and hardness, which is described by the Hall-Petch relation.[1,2] It is a very unique mechanism since other strengthening mechanisms usually lead to an inverse relation between yield strength and fracture toughness.

Grain-boundary (GB) hardening according to the Hall-Petch relation only applies as long as dislocations are produced and can pile up at the grain boundary. After the density of dislocations that can flow freely and pile up against the grain boundaries reaches a certain level, the strengthening potential through a further grain refinement successively decreases, and the Hall-Petch slope decreases. The Hall-Petch behavior for polycrystalline materials has been described by several dislocation models.[3–5] For nanocrystalline metals, a breakdown in the Hall-Petch relation is expected at a critical grain size, where dislocation pileup is no longer supported.[6–8] Moreover, grain-size refinement decreases pining distances preventing dislocations generation by Frank-Read sources. Computer simulations[9–12] have shown that this type of breakdown occurs below a critical grain size (of the order of 10–20 nm for metals) and that instead, plastic deformation occurs by intergranular mechanisms. Also, experimental evidence shows a corresponding change in the cracking pattern and morphology below a critical grain size.[13,14] At the smallest grain sizes, grain-boundary sliding, grain rotation, and grain-boundary triple junction activity have been proposed to account for plastic deformation without dislocation motion.[15–18]

Molecular dynamics techniques have been used in the study of fracture phenomena for many years now. Two-dimensional studies have been performed[19–21] as well as three-dimensional studies.[22,23]

Many studies have been performed in the recent years to explore the particular atomistic processes of crack propagation in α-iron (body-centered cubic structure) single crystals.[24–34] These studies have stressed the effects of temperature and crack orientations on fracture properties for α-Fe single crystal. However, very few results have been published on nanocrystalline α-Fe.[35–37]

In the present study, we explore a mode I fracture behavior in nanocrystalline α-Fe at temperatures ranging from 100 K to 600 K. We address the dual intergranular/intragranular fracture process at such small grain sizes and the effect of temperature on these mechanisms.

II. TECHNIQUES

Atomistic computer simulation and particularly molecular dynamics (MD) simulation is a very useful technique to study the fracture mechanisms in metallic materials.[38–42] The approach is very similar to real experiments and yields detailed information about the deformation and failure mechanisms operating in the simulated systems. For the purposes of the present study, three nanocrystalline samples $S1$, $S2$, and $S3$ corresponding to three different grain sizes (6, 9, and 12 nm, respectively) were geometrically created using the Voronoi construction.[43] In this construction, fully three-dimensional grains are randomly nucleated within a cube. Each grain grows with a random crystallographic orientation until the grains reach one another, generating grain boundaries. The Voronoi construction gives a random nanocrystalline sample with grain-boundary structure similar to what is expected in polycrystalline materials. The three samples created contained 15 grains each and 250 000, 800 000, and 2 000 000 atoms, respectively.

The samples were then relaxed into a minimum-energy nanocrystalline α-Fe structure using molecular statics (MS)

TABLE I. Surface energy values predicted by the potential for various orientations in J/m^2. The energy of a $\Sigma=5$ symmetrical tilt [001](310) grain boundary is also included for comparison.

Orientation	110	100	111	310
Surface energy (J/m^2)	1.43	1.62	1.79	1.64
GB energy (J/m^2)				1.1

and an EAM (embedded atom method) interatomic potential for α-Fe.[44] A comparison of this potential with other interatomic potentials available in the literature can be found in a previous paper.[45] This potential has also been tested previously in MS simulations of crack propagation in α-Fe single crystals.[29] MS is a technique designed to determine the minimum-energy configuration of a given system. Every atom within the simulation block interacts with its surroundings as described by the interatomic interaction potential. Using a conjugate gradient method,[46] the minimization technique, the minimum-energy state is reached through an iterative relaxation process. The total energy and forces on every atom are computed after each iteration and the system is assumed to be at equilibrium when the total energy change and the forces on each atom are below the specified convergence values. The relaxation process yields minimum-energy grain-boundary structures with no differences observed in grain shape or size from the initial construction. Table I reports the values of surface energies for various surface orientations that are given by this potential, using molecular statics relaxation. For comparison, Table I also includes the prediction of the potential for the grain-boundary energy of a symmetrical tilt [001] grain boundary along a (310) plane. The difference in energy between the bcc phase and the fcc phase given by this potential is 0.03 eV.

The grain-boundary structures obtained using the method of sample generation and relaxation described above correspond to random general boundaries. In previous work, the resulting boundaries have been characterized in detail for a similar sample creation algorithm.[47] The main result of that characterization is that the boundaries are not generally amorphous. They consist of ordered regions that are joined by more disordered regions. In many boundaries, the order portions were found to contain structural units typical of special coincident lattice boundaries, whereas the disordered regions accommodate the deviations that the random orientations may have from coincident lattice boundaries.

A semi-infinite mode I crack was introduced in the α-Fe samples using the isotropic elastic approximation. The cracks can be loaded at particular stress intensity values, with the load imposed through displacements that are calculated according to the elastic solution for a mode I semi-infinite crack at the given stress intensity. MS was used to relax the crack tip region to a minimum energy configuration. Periodic boundary conditions are used in the direction of the crack front. The initial crack is an atomically sharp wedge with its tip located near the center of the simulation block. The cracked samples were equilibrated at three different temperatures (100 K, 300 K, and 600 K) using MD for 2000 steps (each step is 8×10^{-15} s). With this technique, the fracture process in each sample was conducted for the three temperatures by incrementally loading the semi-infinite mode I crack starting from a stress intensity value slightly below that given by the Griffith criterion for single crystals ($0.6\ \mathrm{eV/\AA^{5/2}}=0.96\ \mathrm{MPa}\sqrt{m}$). We let the system evolve for 1000 MD steps between each loading (each step is 8×10^{-15} s). The load is kept constant for 1000 MD steps and then increased to the next level. The overall simulation time was 200 ps. Under the stress intensity at a certain temperature, the sample evolves constrained to the equations of motion. The temperature is kept constant using a velocity scaling algorithm. Since the MD technique follows the actual forces on the atoms as they migrate, the fracture mechanisms can be determined by direct observation, without having any *a priori* assumptions. As the simulation progresses and the stress intensity is increased, the crack begins to advance and we follow the crack for a stress intensity up to three times the Griffith value. The simulated strain rate is very high compared to real experiments, as is usually the limitation of the molecular dynamics technique. To address this limitation, we conducted MS simulations of the same samples to compare them with MD simulations at low temperature. Since in the MS technique, the system reaches equilibrium at each loading level these results are representative of low strain rates, where the system has enough time to reach equilibrium. We verified that the same fracture and deformation mechanisms occur using the MS conjugate gradient technique, as observed with MD. The molecular statics technique used is similar to that used previously in studying fracture in nanocrystalline fcc Ni.[48] Even though it is not possible to completely rule out high strain rate effects, the comparison with the conjugate gradient helps establish confidence in the results. We also point out that because of energy release mechanisms other than crack propagation, our simulations result in slow crack growth. The crack velocities that we obtain with our technique are between 10 and 20 m/s.

III. RESULTS

The three samples do not have the same grain size, but their initial geometric structure is the same. In other words, the three samples have the same number of grains (15) and the same grain arrangement, with the same orientation of each grain and grain boundaries; only the grain size differs. This aspect makes comparison between samples more meaningful, by isolating grain-size effects. Observation inside the sample is made possible by digitally cutting the sample into slices perpendicular to the crack front line. Therefore, the atomic structure and fracture process in each sample is studied by exploring a collection of different slices taken at various levels along the crack front line. In order to compare the three samples, the slices have to be at the same corresponding location. To clearly represent the atomistic structure of the samples, a shading code associated with the atomic arrangement of the atoms is adopted. Three different shades of gray are assigned to atoms in perfect bcc arrangement (8-coordinated atoms), atoms with less than eight neighbors and atoms with more than eight neighbors. The number of neighbors is calculated within a distance of 0.27 nm, and the non-

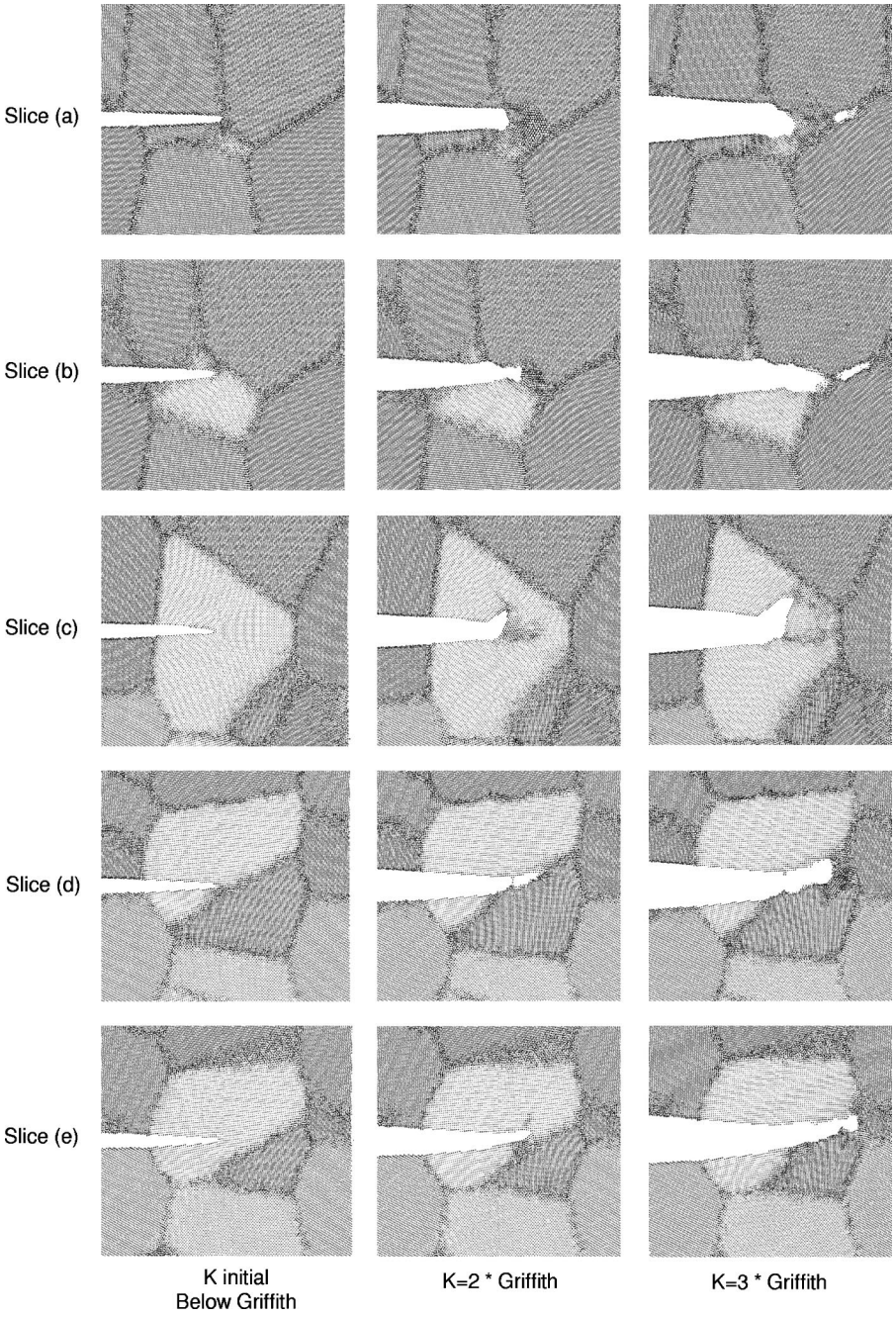

FIG. 1. Intragranular/Intergranular fracture in $S3$ (12 nm grain size) at 100 K: slices at different positions along the crack front line at loadings of just below the Griffith value, two times the Griffith value, and three times the Griffith value. The darker shades of gray represent atoms that have nonperfect coordination.

perfectly coordinated atoms are given darker shades of gray. This procedure allows us to distinguish grain boundaries from the inner part of the grains, with atoms in perfect bcc arrangement, and also reveals eventual defects due to deformation and fracture mechanisms.

Initially, the crack tip is situated at the center of the cubic shaped sample. This somewhat artificially introduced crack has its crack front edge ending in different positions with respect to the grain boundaries. Therefore, the crack tip starts in the inner region of grains, at grain boundaries, or at grain-boundary triple junctions. These different configurations influence the crack propagation. The incremental mode I loading is applied to the three samples at three different temperatures. Observations at an atomic scale enable us to explore the different mechanisms of the fracture process as well as the effect of temperature and grain size. The fracture process is found to occur mainly as an intergranular fracture process combined with various deformation mechanisms. Temperature and grain size are found to highly influence the combination of fracture and deformation mechanisms that operate.

A. Intragranular/Intergranular fracture process

Figure 1 represents a selection of slices along the crack front line of the 12 nm sample $S3$, at different stress intensities. This figure allows us to observe the combined intragranular/intergranular fracture process at 100 K. In this and subsequent sample slices we calculated the number of neighbors up to a distance of 0.27 nm. If this number is not

TABLE II. Number of dislocations observed in four different slices of the 9 nm grain-size sample at 100 K and the expected crack blunting due to these dislocations, compared with the observed blunting.

Slice level (nm)	0	−2	−6	−8	Average	Expected blunting (nm)	Observed blunting (nm)
Number of Dislocations	6	6	6	5	5.75	0.8	1.4

equal to 8 (the perfect lattice coordination for the bcc structure), the atoms are represented in a darker shade of gray. As it can be seen in this figure, the initial crack front line ends at different locations in the structure with respect to grain boundaries. The crack tip starts in the inner region of grains [slice (c) and (e)], at grain boundaries [slice (b) and (d)], or at grain-boundary triple junctions [slice (a)]. These different initial configurations influence the crack propagation.

Slices (c) and (e) enable us to observe directly the intragranular fracture process, due to the fact that the initial position of the crack in these slices is near the center of a grain. Therefore, in the case of slices (c) and (e), the crack starts far from a grain boundary and propagates intragranularly until it reaches a grain boundary. With increased loading, the crack propagates in a different manner depending on the crystallographic orientation of the grain and the temperature of the simulation. For intragranular propagation, as the sample is loaded, the crack deviates to the most favorable crystallographic orientation, which corresponds to the lowest surface energy. For this potential this is the {110} type surface, with a surface energy of 1.43 J/m^2 (Table I) An example of this is seen in slice (c), where the crack was initially oriented with {100} type crack faces. The crack deviates as soon as it is loaded to propagate along the lowest surface energy {110} type plane. The intragranular fracture process is also observed in slice (e). In this slice, the grain is oriented so that the crack plane already lies close to the lowest surface energy orientation. The increase in loading causes the crack to propagate in a straight direction without any blunting. The crack remains atomically sharp and no dislocations are observed. A brittle behavior is observed at low and high temperature. In both configurations, the crack keeps advancing until it reaches a grain boundary. In both configurations of slices (c) and (e), the crack keeps propagating and eventually reaches a grain boundary. At that point, the fracture enters an intergranular mode.

The propagation of the crack is associated with some degree of crack blunting and dislocation activity even at low temperature. The origin of the localized plasticity associated with blunting of the crack is complex. In bcc metals, dislocations do not leave any stacking fault behind them as in fcc metals. In the study of nanocrystalline fcc materials[48] the stacking faults were used in the visualization of dislocation activity. In the bcc lattice there are no stacking faults and in the present case the visualization of dislocations is more difficult. Nevertheless, it is possible to detect and follow the emitted dislocations by constructing Burgers circuits as the sample is loaded. These dislocations are present at the three temperatures 100 K, 300 K, and 600 K. The dislocations are seen to travel from the crack tip region through the grains towards a neighboring grain boundary. For the 9 nm sample loaded at 100 K, we monitored the number of dislocations emitted as the sample was loaded using four different slices, taken at different levels along the crack front. This was done in order to compare the blunting produced by the observed dislocations with the total blunting observed in the crack, and the results are shown in Table II.

We found that as the sample was loaded up to three times the Griffith load, 5 to 6 dislocations were emitted, depending on the location of the slice studied. We estimate that each dislocation of $\frac{1}{2}\langle 111\rangle$ Burgers vector, when projected perpendicular to the crack surfaces should cause an average blunting of about half the lattice parameter or 0.14 nm. The total blunting expected from the dislocations observed is therefore approximately 0.8 nm. This number can be compared with the actual blunting observed for this sample of 1.3 to 1.5 nm. This comparison suggests that not all the blunting observed can be attributed to dislocation mechanisms. The additional blunting produced can be attributed to other mechanisms. These may include grain-boundary accommodation mechanisms and new grain formation. This latter mechanism is discussed in detail in recent paper by us.[49] The mechanisms of plastic deformation at such small grain sizes are thought to be different than the regular dislocation based deformation process for conventional size polycrystalline metals. At these extremely small grain sizes other phenomena, such as grain-boundary sliding, grain rotation, and grain-boundary triple junction activity, are proposed to account for plastic deformation. Indeed, the crack propagation in slice (c) is associated with a stress induced grain nucleation at the crack tip that accounts for plastic energy release. This process occurs through the formation of a metastable compact phase, possibly aided by the high local pressures present at the crack tip. This mechanism of grain nucleation at the crack tip resembles that reported recently in Fe by Holian *et al.*[50] and was analyzed in detail in a separate study using the same potential and the same sample configurations as the present work.[49]

The intergranular fracture initiation and propagation depends on the configuration crack/grain boundary orientation as well as temperature. When the crack reaches a grain boundary, it does so in different crack/grain boundary configurations, as we see in slice (a), (b), and (d) of Fig. 1. In slice (a), the grain-boundary is nearly perpendicular to the crack propagation direction. However, in slice (b) and (d), the angle between the grain boundary and the crack propagation direction is smaller. In slice (a) crack arrest along with significant blunting occurs after increasing stress intensity to twice the Griffith value. For the same stress intensity, a crack propagation along the grain boundary is observed for the two other slices (b) and (d). In slice (a), as the stress intensity is increased the crack tip keeps blunting without crack propagation. Eventually, when the stress intensity reaches a certain level, a nanovoid is created ahead of the blunted crack in a

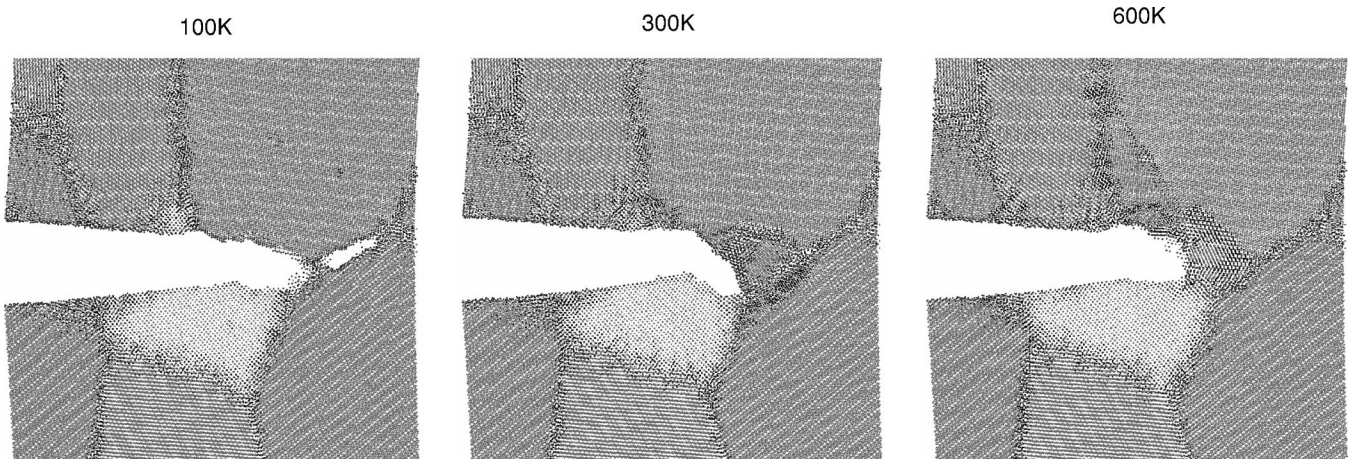

FIG. 2. Temperature effect on crack propagation in slice (b) of $S3$ (12 nm grain size) at the maximum loading (a stress intensity factor equal to three times the Griffith value). The darker shades of gray represent atoms that have nonperfect coordination.

grain-boundary region more favorably oriented, forming a smaller angle with the crack propagation direction. At later stages, these nanovoids join the main crack. In slice (b) and (d), the grain boundaries are oriented close to the crack propagation direction and the crack advances intergranularly as the stress is increased. When the crack reaches a nearly perpendicular grain boundary, the same scenario as in slice (a) occurs and a nanovoid is created ahead of the blunted crack. This phenomenon occurs in slice (b) and the crack propagates in the favorably oriented grain boundary ahead of the crack tip. In slice (d), crack arrest occurs further to the right of the sample and the same scenario would occur as the stress intensity is increased. By measuring the angles between grain boundaries and crack plane in various slices, we can deduce simple conditions for crack propagation or crack arrest due to grain-boundary orientation. Indeed, for angles between 0 and about 45°, we observe crack propagation along the grain boundary. On the other hand, for angles between 75° and 90°, crack arrest is observed.

B. Effect of temperature

Figure 2 compares slice (b) of the largest grained sample $S3$ at the three temperatures for the maximum loading simulated. The effect of temperature is the same for all the different slices, therefore only slice (b) is presented. It is clear that the increase in temperature from 100 K to 600 K causes more blunting at the crack tip and more crack arrest. At low temperature (100 K), the crack has propagated along the grain boundary. At higher temperature (300 K), the crack still propagates along the grain boundary, but the increase in ductility does not enable the crack to propagate as much. Finally, at the highest temperature tested (600 K), the blunting of the crack is more pronounced and crack arrest is observed at the boundary. We can also observe that at 300 K and 600 K, the crack propagation is associated with grain nucleation at the crack tip accounting for plastic energy release. At higher temperatures, with increasing stress intensity nanovoids will eventually be formed ahead of the crack tip and the crack will propagate along the grain boundary. Hence, higher stress intensity is needed to initiate intergranular fracture at higher temperatures. The same trend is observed for the two other, smaller grained samples, $S1$ and $S2$. With increasing temperature, the atomic vibrations increase causing atoms to move more easily when subjected to loading. Thus, at higher temperature plastic deformation becomes easier and crack blunting occurs. From these atomistic observations, fracture resistance is increased with increasing temperature, as expected.

C. Energetics of crack propagation

By following the excess potential energy of the simulation block as a function of crack advance, we can introduce a simple method to obtain the critical energy release rate G_{IC}, which can be directly related to the fracture toughness K_{IC} through classical fracture mechanics. G_{IC} represents the resistance to crack propagation, i.e., the energy per surface area that is needed to open the crack. For instance, in a perfectly brittle material, G_{IC} would be equal to twice the surface energy. Figure 3 shows the excess energy of the simulation block per unit length of crack front, plotted as a function of the average crack propagation distance for $S3$ (12 nm grain size). The figure illustrates the effect of the three temperatures (100 K, 300 K, and 600 K) on G_{IC}. G_{IC} is given by the slope of each curve. Thus, the slope of each curve represents the average fracture resistance of α-Fe at temperatures 100 K, 300 K, and 600 K. These slopes have been calculated as an average over the entire range of the crack propagation distance. Table III summarizes the values for G_{IC} obtained from the average slopes for the three different temperatures simulated. It is clear that the fracture resistance increases with temperature. This result is not surprising and can be associated with an increase in plasticity with temperature, which has been illustrated in the previous observations. With increasing temperature, the atomic vibrations increase and the atoms move more easily enabling more plastic deformation in the structure.

D. Effect of grain size

Figure 4 illustrates the same equivalent slices as in Fig. 1 for the three samples $S1$, $S2$, and $S3$ (grain sizes of 6, 9, and

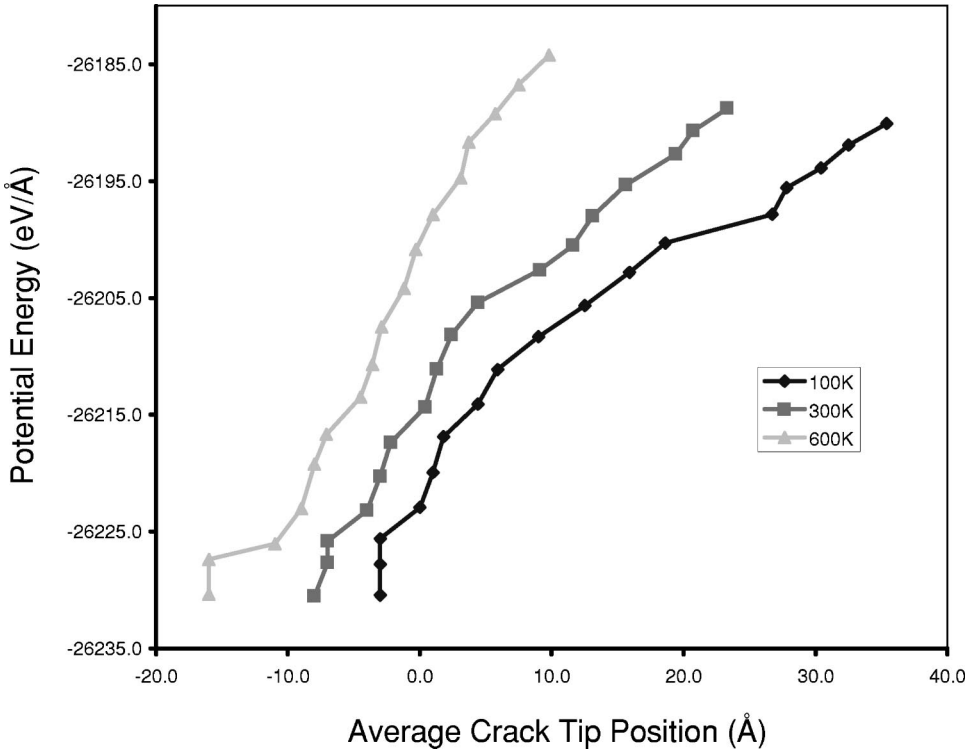

FIG. 3. Excess potential energy vs average crack advance for $S3$ (12 nm grain size) at 100 K, 300 K, and 600 K.

12 nm, respectively) at the maximum loading of the simulation (three times the Griffith value for single crystal) and at 100 K. From the figure, we can clearly see that at the same maximum loading the average crack front has advanced more for the larger grained sample. In the three samples, the crack has propagated in a mixed intragranular/intergranular fracture process described in the previous sections. For the larger grained sample, the crack progress is associated with further propagation along the grain boundaries by void nucleation and grain nucleation within certain grains. As the grain size is decreased, the volume fraction of grain boundaries increases and blunting and crack arrest become more important. From atomistic observations at such small grain sizes, we see that fracture resistance is lowered with increasing grain size. As the grain size is decreased, blunting of the crack tip becomes more important and fracture resistance increases. The resistance to fracture can be estimated by the Wells-Cottrell concept of critical crack opening displacement (COD) at the crack tip during fracture.[51,52] From direct observation, the COD at the crack tip can be estimated for the three samples $S1$, $S2$, and $S3$ (grain sizes of 6, 9, and 12 nm, respectively). Practically, the COD for each sample is estimated by considering a collection of slices along the crack front line and averaging the COD values measured at the atomistic scale. The COD for the largest grained sample $S3$ has been estimated to be 16 ± 3 Å, whereas the intermediate grain-size sample $S2$ it is 14 ± 4 Å, and for the smallest grained sample $S1$ it is 9 ± 2 Å. Figure 5 illustrates the effect of grain size on the COD for the three samples at 100 K. It can be seen that the COD at the crack tip, i.e., fracture resistance, increases with decreasing grain size. From these results, we observe an increase in fracture resistance with decreasing grain size in nanocrystalline α-Fe. Therefore, we obtain the same trend as for conventional grain-size polycrystalline materials, where fracture toughness is also observed to increase with decreasing grain size. However, the mechanisms responsible for the increase in fracture toughness with decreasing grain size may not be the same in the coarse-grained polycrystalline material and in the nanocrystalline material. Grain-boundary arrest of the crack is a common effect at both scales, but in conventional grain sized polycrystals, dislocation activity is a main mechanism associated with plasticity that is not present in the nanocrystalline material. Instead, other mechanisms such as grain-boundary accommodation, grain-boundary triple junction activity, grain nucleation, and grain rotation dictate the plastic energy release mechanisms at the nanoscale. We have also analyzed the effects of grain size on the dynamics of grain propagation and we have found that as the grain size increases, the velocity of crack propagation increases. In the simulations presented here the average crack velocities at 100 K increase from 14 m/s for the smallest grained sample to 19 m/s for the largest grained sample. A similar increase was observed at 600 K from 10 to 13 m/s.

TABLE III. Dependence of the fracture energy on temperature for $S3$ (12 nm grain size), in ev/nm^2.

Temperature (K)	100	300	600
G_{IC} for 12 nm grains	94 eV/nm^2	129 eV/nm^2	194 eV/nm^2

IV. CONCLUSIONS

In this study, we used computer-simulation techniques to explore the fracture and deformation behavior in nanocrys-

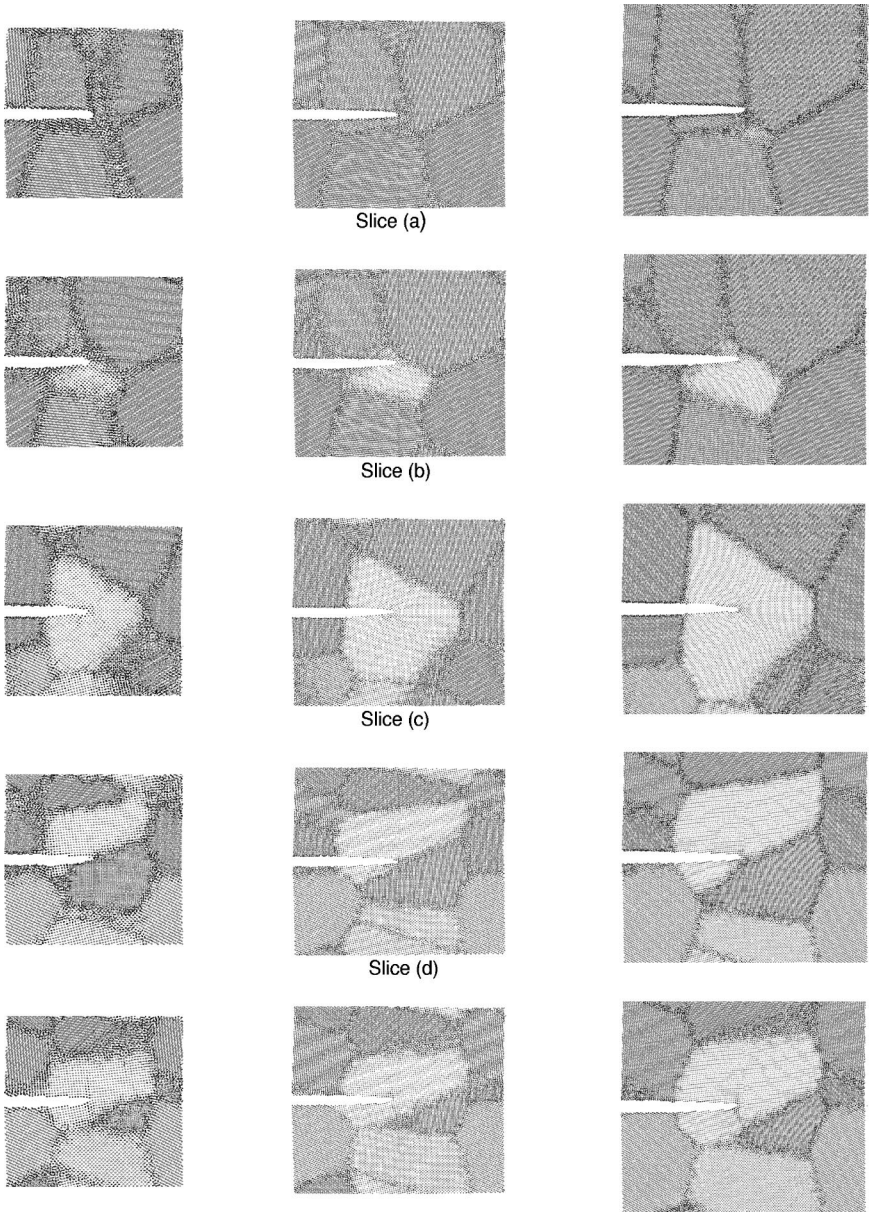

FIG. 4. Slices at different positions along the crack front line of the three different samples $S1$ (6 nm grain size), $S2$ (9 nm grain size), and $S3$ (12 nm grain size) at a stress intensity factor equal to three times the Griffith value and 100 K. The darker shades of gray represent atoms that have nonperfect coordination.

talline α-Fe at temperatures ranging from 100 K to 600 K. The fracture process was conducted using molecular dynamics for three samples corresponding to three different grain sizes 6, 9, and 12 nm. The fracture behavior in each sample was followed directly at the atomic scale by incrementally loading a mode I crack to high stress intensities.

The fracture process in nanocrystalline α-Fe is observed to occur as an intragranular fracture process combined with an intergranular fracture process. Intragranular fracture is dependent on crystallographic orientation. If the crystal is favorably oriented, the crack propagates in a brittle manner even at high temperature. On the other hand, crack deviation is associated with plastic deformation. We observe dislocations at the tip of the crack for the three temperatures tested, but not enough to account for the blunting. At such small grain sizes, the mechanisms of plastic deformation are thought to occur by grain-boundary accommodation, grain rotation, and grain-boundary triple junction activity rather than dislocation-based mechanisms. A stress induced mechanism accounting for the plastic deformation at the crack tip will be studied in detail in a separate work. Intergranular fracture is found to be highly dependent on the grain-boundaries orientations. If the angle between the grain boundary and the crack plane is below 45°, crack propagation along the grain boundary is observed. However, if the angle is larger than 75°, crack arrest occurs. Between these two critical angles, a combination of the two mechanisms is believed to occur. In the case of crack arrest, with increasing stress intensity, intergranular fracture proceeds by the coalescence of nanovoids formed in more favorably oriented grain boundaries ahead of the crack.

Temperature and grain size are found to highly influence the fracture mechanisms. From direct observations of the fracture process, it is clear that the increase in temperature causes more blunting and crack arrest. We also observe more grain nucleation sites associated with crack propagation at

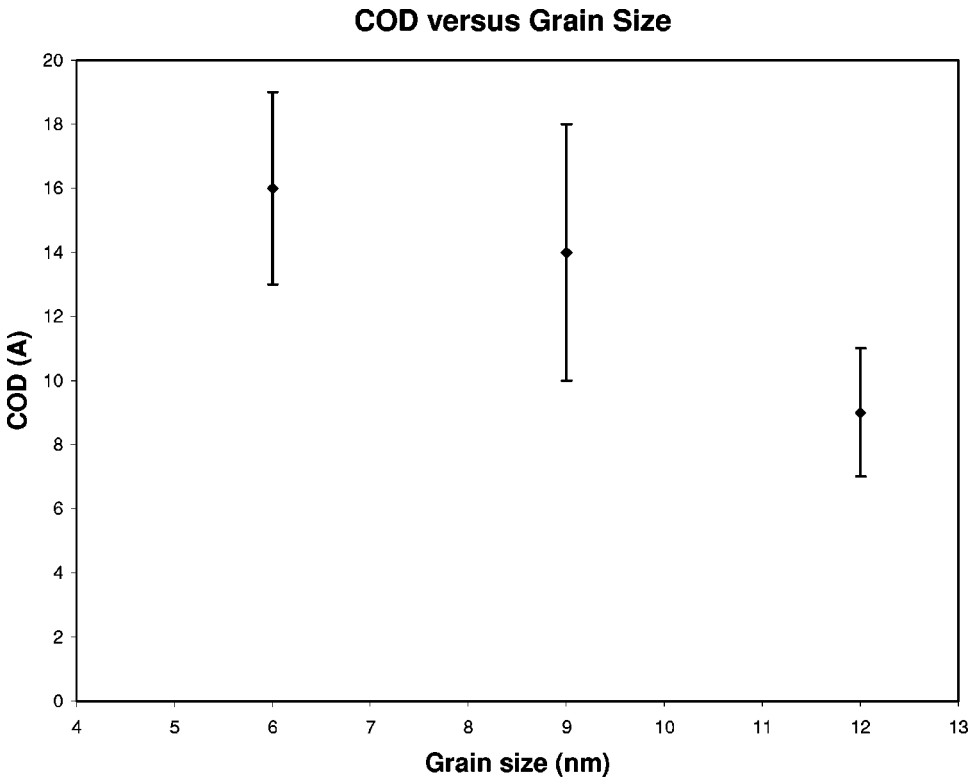

FIG. 5. Crack opening displacement (COD) at the crack tip versus sample grain size at 100 K and a loading equal to three times the Griffith value.

higher temperatures. From energy consideration, the overall average fracture resistance is found to increase with increasing temperature. For the larger grain size (12 nm), the overall critical energy release rate (G_{IC}) is equal to 94 eV/nm^2 at 100 K. This value can be directly related to fracture toughness (K_{IC}) using plain-strain classical fracture mechanics equation. K_{IC} is equal to 1.05 eV/Å$^{5/2}$(1.7 M Pa$\sqrt{m}$). This value corresponds to the critical stress intensity for the onset of crack propagation in $S3$ (12 nm grain size) at 100 K. Similarly, we obtain K_{IC} equal to 1.23 eV/Å$^{5/2}$(1.97 M Pa$\sqrt{m}$) at 300 K. In polycrystalline α-Fe with conventional grain sizes (10–300 μm), the fracture toughness is between 450 and 500 M Pa$\sqrt{m}$ at room temperature.[53] The lower values obtained for fracture toughness in the nanocrystalline material can be explained by the change in plastic mechanisms from conventional to nanograin sizes. For the nanocrystalline material, dislocation activity is not the main mechanism accounting for plastic deformation. Instead, grain-boundary accommodation, grain-boundary triple junction activity, grain nucleation, and grain rotation dictate the fracture behavior. Hence, plastic energy release mechanisms are not the same for the polycrystalline and the nanocrystalline material, which result in lower values for fracture toughness in nanocrystalline α-Fe. In addition, although dislocations are not believed to be the main mechanisms for plastic deformation in nanocrystalline materials, no dislocation sources are present in our simulations (no preexisting dislocations, no impurities) that would allow more dislocation activity and an increase in fracture toughness for the same grain sizes studied. Furthermore, in our simulations, grain-boundary fraction is found to highly influence crack propagation and fracture toughness is observed to increase with decreasing grain size. This trend parallels the increase in fracture toughness with decreasing grain size observed in conventional size polycrystalline material. For the smaller grain sizes, the large number of grain boundaries causes blunting and crack arrest. The effect of grain size on fracture resistance is estimated by the crack tip opening displacement, which increases with decreasing grain size.

The use of molecular dynamics was motivated by the ability of the technique to reproduce the physical behavior of the system. Since the MD technique follows the actual forces on the atoms as they migrate, the fracture mechanisms can be determined by direct observation, without having any *a priori* assumptions. However, it is important to stress that the quantitative accuracy of this technique, as well as the MS technique, is limited by that of the potentials used.

ACKNOWLEDGMENTS

This work was supported by the office of Naval Research, Division of Materials Science (Grant No. N00014J-1351). The authors would like to thank Helena van Swygenhoven for help in creating the digital samples and valuable discussion.

[1] E.O. Hall, Proc. Phys. Soc. London, Sect. B **64**, 747 (1951).
[2] N.J. Petch, J. Iron Steel Inst., London **174**, 25 (1953).
[3] A.H. Cottrell, Trans. AIME **212**, 192 (1958).
[4] J.C.M. Li, Trans. AIME **227**, 239 (1963).
[5] M.A. Meyers and E. Ashworth, Philos. Mag. A **46**, 737 (1982).
[6] C.C. Koch, D.G. Morris, K. Lu, and A. Inoue, MRS Bull. **24**, 54 (1999).
[7] J.R. Weertman, D. Farkas, K. Hemker, H. Kung, M. Mayo, R. Mitra, and H. Van Swygenhoven, MRS Bull. **24**, 44 (1999).
[8] R.A. Masumura, P.M. Hazzledine, and C.S. Pande, Acta Mater. **46**, 4527 (1998).
[9] H. Van Swygenhoven and A. Caro, Appl. Phys. Lett. **71**, 1652 (1997).
[10] J. Schiotz, F.D. Di Tolla, and K.W. Jacobsen, Nature (London) **391**, 561 (1998).
[11] H. Van Swygenhoven and A. Caro, Phys. Rev. B **58**, 11 246 (1998).
[12] A. Hasnaoui, H. Van Swygenhoven, and P. M. Derlet, Phys. Rev. B **66**, 184112 (2002).
[13] T.R. Malow and C.C. Koch, Metall. Mater. Trans. A **29**, 2285 (1998).
[14] T.R. Malow and C.C. Koch, Acta Mater. **46**, 6459 (1998).
[15] J. Schiotz, F. Di Tella, and K. Jacobson, Nature (London) **391**, 561 (1988).
[16] H. Van Swygenhoven, M. Spaczer, and A. Caro, Acta Mater. **47**, 3117 (1999).
[17] H. Hahn and K.A. Padmanabhan, Philos. Mag. B **76**, 559 (1997).
[18] G. Palumbo, U. Erb, and K. Aust, Scr. Metall. Mater. **24**, 2347 (1990).
[19] W.T. Ashurst and W.G. Hoover, Phys. Rev. B **14**, 1465 (1976).
[20] B.L. Holian and R. Ravelo, Phys. Rev. B **51**, 11 275 (1995).
[21] B.L. Holian, A.F. Voter, N.J. Wagner, R.J. Ravelo, S.P. Chen, W.G. Hoover, C.G. Hoover, J.E. Hammerberg, and T.D. Dontje, Phys. Rev. A **43**, 2655 (1991).
[22] S.J. Zhou, P.S. Lomdahl, A.F. Voter, and B.L. Holian, Eng. Fract. Mech. **61**, 173 (1998).
[23] M. Marder and J. Fineberg, Phys. Today **49** (9), 24 (1996).
[24] K. Nishimura and N. Miyazaki, CMES-Comput. Mode. Eng. Sci., **2**, 143 (2001).
[25] K. Cheung and S. Yip, Modell. Simul. Mater. Sci. Eng. **2**, 865 (1994).
[26] K. Cheung, R.J. Harrison, and S. Yip, J. Appl. Phys. **71**, 4009 (1992).
[27] B. deCelis, A. Argon, and S. Yip, J. Appl. Phys. **54**, 4864 (1983).
[28] S. Kohlhoff, P. Gumbsch, and H.F. Fischmeister, Philos. Mag. A **64**, 851 (1991).
[29] V. Shastry and D. Farkas, Modell. Simul. Mater. Sci. Eng. **4**, 473 (1996).
[30] A. Machova, G.E. Beltz, and M. Chang, Modell. Simul. Mater. Sci. Eng. **7**, 949 (1999).
[31] K. Ogawa, Philos. Mag. **11**, 217 (1965).
[32] M. Mullins, Acta Metall. **32**, 381 (1984).
[33] V. Vitek, Scr. Metall. **4**, 725 (1970).
[34] N. Yanagida and O. Watanabe, JSME Int. J., Ser. A **39**, 321 (1996).
[35] H. Inoue, Y. Akahoshi, and S. Harada, Mater. Sci. Res. Int. **1**, 95 (1995).
[36] D. Chen, Mater. Sci. Eng., A **190**, 193 (1995).
[37] Z. Chen, J. Ding, Nanostruct. Mater. **10**, 205 (1998).
[38] D. Farkas, MRS Bull. **25**, 38 (2000).
[39] S.J. Zhou, D.M. Beazley, P.S. Lomdahl, and B.L. Holian, Phys. Rev. Lett. **78**, 479 (1997).
[40] K.S. Cheung and S. Yip, Phys. Rev. Lett. **65**, 2804 (1990).
[41] R.K. Kalia, A. Nakano, A. Omeltchenko, K. Tsuruta, and P. Vashishta, Phys. Rev. Lett. **78**, 2144 (1997).
[42] D. Farkas, Philos. Mag. Lett. **80**, 229 (2000).
[43] G. Voronoi, J. Reine Angew. Math. **134**, 199 (1908).
[44] G. Simonelli, R. Pasianot, and E. Savino, Mater. Res. Soc. Symp. Proc. **291**, 567 (1993).
[45] D. Farkas, S.J. Zhou, C. Vailhe, B. Mutasa, and J. Panova, J. Mater. Res. **12**, 93 (1997).
[46] J.E. Sinclair and R. Fetcher, J. Phys. C **7**, 864 (1972).
[47] H. Van Swygenhoven, D. Farkas, and A. Caro, Phys. Rev. B **62**, 831 (2000).
[48] D. Farkas, H. Van Swygenhoven, and P. Derlet, Phys. Rev. B **66**, 060101 (2002).
[49] A. Latapie and D. Farkas, Modell. Simul. Mater. Sci. Eng. **11**, 745 (2003).
[50] K. Kadau, T.C. Germann, P.S. Lohmdahl, and B.L. Holian, Science **296**, 1681 (2002).
[51] A. H. Cottrell, I. S. I. Special Report No. 69, 1961 (unpublished).
[52] A. A. Wells (unpublished).
[53] Z. Fan, Mater. Sci. Eng., A **191**, 73 (1995).